RESEARCH ARTICLE

Surface Area Measurement of Irregular Objects Based on 3D Laser Scanning Technology

Quan Qi[1,*], **Yuhua Wang**[1], **Xingdong Wang**[1] **and Lulu Shi**[1]

[1] College of Information Science and Engineering, Henan University of Technology, Zhengzhou 45001, China

Abstract

Calculating surface area is quite common in daily life; however, due to the irregular shapes of objects, traditional feature point data collection methods are not suitable for complex surfaces. Therefore, this study employs 3D laser scanning technology, using the Ligrip H120 handheld rotating laser scanner for data collection of the artificial stone. Based on four algorithms, we performed 3D reconstruction of the obtained point cloud data. Subsequently, we developed a program for surface area calculation using the Python interface of CloudCompare software and the Open3D library. The results indicate that the surface area measured with this technology has an accuracy improvement of 1.03 percentage points compared to the traditional sticker method, while the time required was reduced by three-quarters. This technology demonstrates high precision, strong reliability, and high efficiency in calculating the surface area of irregularly shaped objects.

Keywords: 3D laser scanning, irregular objects, surface area, Ligrip H120, 3D reconstruction algorithms.

Academic Editor:
Jinchao Chen

Submitted: 28 October 2024
Accepted: 27 November 2024
Published: 11 December 2024

Vol. 1, **No.** 2, 2024.
10.62762/TIUS.2024.725258

***Corresponding author:**
✉ Quan Qi
435995612@qq.com

1 Introduction

As the process of urbanization accelerates, urban landscape architecture has increasingly gained attention and importance as a green calling card of cities. Among various landscape elements, the artificial rockery, or simulated stone mountain, has become an indispensable part due to its unique charm and characteristics. Depending on the method of construction, artificial rockeries can be categorized into earthen mounds, stone assemblages, and simulated stone mountains. Among these, simulated stone mountains are particularly favored due to their advanced manufacturing techniques and notable advantages. They utilize high-strength reinforced concrete as a foundation, combined with meticulously designed steel truss structures, resulting in a robust and high-load-bearing internal framework. Additionally, cement mortar is employed to intricately shape the exterior, accurately mimicking the textures and forms of natural rock formations.

However, the complex surfaces of simulated stone mountains often render traditional area measurement methods ineffective in capturing their detailed features, leading to measurement errors. Given that the cost can reach hundreds to thousands of yuan per square meter, this can provoke disputes among stakeholders in the project. Consequently, the application of 3D laser scanning technology offers a novel solution for the precise measurement of the surface area of artificial rockeries. Esteemed as an advanced measurement method known as "real-scene

Citation
Qi, Q., Wang, Y., Wang, X., & Shi, L. (2024). Surface Area Measurement of Irregular Objects Based on 3D Laser Scanning Technology. *IECE Transactions on Intelligent Unmanned Systems*, 1(2), 63–72.

replication technology," 3D laser scanning can swiftly and accurately capture the 3D data of target objects and construct high-precision 3D models. By integrating with GPS technology, this method achieves efficient and accurate field measurements.

3D laser scanning technology emerged in the 1960s, initially focusing on the development of airborne mapping techniques. In the 1990s, significant advancements in accuracy and efficiency led to its prominence as a focal point of research within the surveying discipline. El-Hakim et al. [1] developed an indoor scene modeling scanning platform that integrated 3D laser scanners with CCD cameras. Lemmens [2] performed 3D scanning on Michelangelo's David, demonstrating the immense application value of this technology in fields such as cultural heritage preservation. Subsequently, 3D laser scanning technology has steadily advanced toward industrialization.

Yu et al. [3] conducted research on indoor scene simulation to meet architectural demands. Allen et al. [4] established a foundational study for realistic 3D building models through camera technology. In the same year, an Austrian company utilized this technology to perform detailed scans of the Alps, providing invaluable data support for geological research and environmental monitoring.

Domestic research on 3D laser scanning technology is also extensive. The Tianyuan OKIO series ground-based 3D laser scanners, independently developed by Beijing Tianyuan, have achieved remarkable success in model reconstruction and industrial design, earning widespread recognition within the surveying community [5]. Zhao et al. [6] applied mobile 3D laser measurement technology to monitor the structural integrity of subway tunnels, developing an efficient method to quickly obtain the 3D geometric features of underground spaces. Zhao et al. [7] acquired 3D point cloud data of underground artifacts in the Tongzhou District of Beijing through 3D laser scanning technology, constructing complete 3D models. Ellmann et al. [8] analyzed the real-time, rapid, and high-precision characteristics of mobile 3D laser scanning technology.

Parfenov et al. [9] explored the practical applications of 3D laser scanning technology in measuring the surface areas of urban sculptures, providing a solid theoretical foundation for the precise measurement of irregularly shaped structures. Dawei et al. [10] validated the high efficiency of 3D laser scanning technology in surface area calculations for mining engineering, particularly highlighting its advantages in large-scale area measurements.

In recent years, as the understanding of 3D scanning technology deepens and the technology itself rapidly develops, an increasing number of researchers and professional engineers have joined this field. Significant and rapid advancements have been made in both the academic and commercial sectors in China, continually catching up with the most advanced technologies and applications internationally. In certain disciplines and research directions, some have even reached a leading global level. Corresponding technological products and achievements have emerged, such as the automation of rapid navigation and positioning for robots using 3D laser scanning technology at the School of Information Engineering, Zhejiang University. Additionally, a joint research and development center was established between Northwestern Polytechnical University and the French company MENSI to conduct research on 3D information acquisition for large industrial and complex scenes, demonstrating the vast application potential of 3D laser scanning technology.

The application of 3D laser scanning technology significantly enhances work efficiency, reduces the volume and intensity of outdoor measurement tasks, improves measurement accuracy, and provides new means and methods for quality and cost management in the construction of simulated stone mountains in landscape engineering

2 Technical principles and data collection

2.1 Principles and methods of surface area measurement

Laser ranging is achieved by measuring the time delay or phase shift of the reflected laser pulse. Using the point cloud data obtained, mathematical modeling techniques can be applied to generate a functional representation of the object's surface, thereby enabling accurate calculation of its surface area [11].

To accurately measure the surface area of the target object, the primary task is to collect dense point cloud data from the object's surface using specific technological means. Subsequently, mathematical functions can be employed to partition the surface into triangular or quadrilateral meshes, and by statistically evaluating the areas of these meshes, the surface area of the target object can be determined. Given that the point cloud data obtained from 3D laser scanning is

discrete, surface fitting processing is required to ensure accurate application in surface area calculations [12].

Let the planar projection area corresponding to the target surface be denoted as Ω, which can be expressed as follows:

$$z = f(x, y),\ (x, y) \in \Omega \tag{1}$$

We divide Ω into a series of square sub-regions $\Omega_{i,j}$, where $i = \{0, 1, \ldots, N\}$; $j = \{0, 1, \ldots, M\}$. The coordinates of the four vertices of each small square are given by $(x_{i,j}, y_{i,j}), (x_{i,j} + d, y_{i,j}), (x_{i,j}, y_{i,j} + d), (x_{i,j} + d, y_{i,j} + d)$. Here, $x_{i+1} = x_i + d; y_{i+1} = y_i + d$, where d represents the mesh size. The z-values of the four corner points of the mesh are denoted as $z_{i,j}, z_{i+1,j}, z_{i,j+1}, z_{i+1,j+1}$. A bilinear interpolation function can be constructed as follows:

$$\begin{aligned} Z = (1-u)(1-v)z_{i,j} + u(1-v)z_{i+1,j} \\ + v(1-u)z_{i,j+1} + uvz_{i+1,\,j+1} \end{aligned} \tag{2}$$

2.2 Data collection from 3D laser scanning

2.2.1 *Data acquisition process*

This study focuses on the landmark plastic rock of Henan University of Technology, exploring the application of 3D laser scanning technology for measuring the surface area of the plastic rock. It further elucidates the significant implications and value of 3D laser scanning technology in the measurement of surface areas of irregularly shaped objects.

Through field investigations, it was observed that the surface of the rock exhibited irregular shapes, as shown in Figure 1. To efficiently and accurately acquire engineering data, a handheld 3D laser scanner was employed for the operation.

Figure 1. Real scene of plastic rock.

The main workflow for the 3D laser scanning operation of the plastc rock is illustrted in Figure 2.

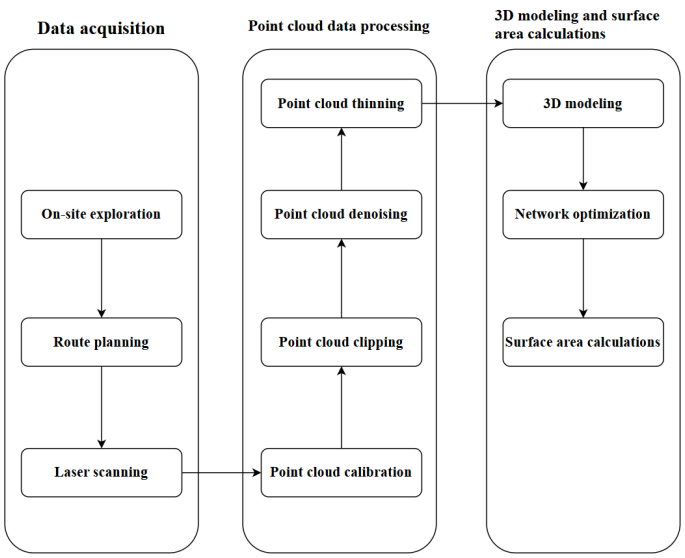

Figure 2. Workflow for surface area study of plastic rock.

2.2.2 *Field Operations*

Field data acquisition is crucial for subsequent data processing, ensuring high-quality point cloud data, thereby reducing the workload of data processing and enhancing the accuracy of the 3D modeling of the plastic rock. Therefore, it is essential to strictly adhere to the established scanning procedures. Detailed scanning steps:

(1) Initialization of the scanner

Before initiating the scan, the scanner must be initialized to ensure data accuracy.

(2) Determination of scanning horizontal position

Based on the results of the field investigation, the optimal scanning location should be identified, and the scanner should be set up to ensure that the scanned area falls within a reasonable range.

(3) Setting scanning parameters

Appropriate scanning resolution should be chosen based on the scanning accuracy and the distance from the object being measured.

(4) Execution of scanning

Once the scanning parameters are set, the scanner is activated to perform an automatic scan of the target object, acquiring the necessary point cloud data.

(5) Acquisition of plastic rock photographs

After completing the scan of the plastic rock, digital photographs should be taken using either a digital camera or a high-resolution smartphone to

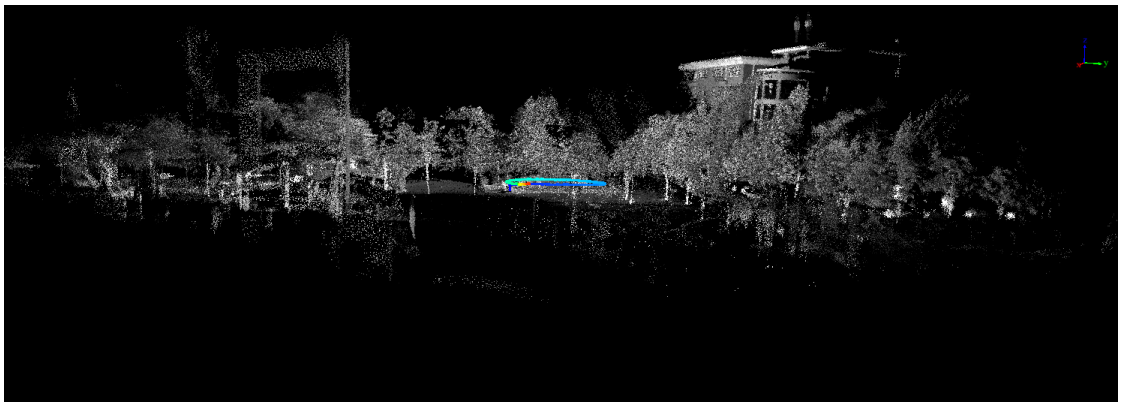

Figure 3. Results of Lifuser-BP software processing.

perform orthometric measurements of the rock's surface, thereby establishing a spatial matching relationship between the plastic rock model and the collected images.

2.2.3 Point cloud data processing

Lifuser-BP, a self-developed point cloud processing software for digital green earth laser radar, supports data processing from various models of laser radar and can also integrate image data to generate colored point clouds. Additionally, it can be quickly integrated into third-party software to support user-defined hardware platforms for data acquisition and processing.

To complete the point cloud data processing, specific IP addresses need to be configured, and the ".bag" files from the share folder must be accessed. In the engineering settings, the following parameters should be adjusted:

Voxel Filtering: The density of the processed point cloud data under default conditions is relatively sparse, approximately 3000–5000 points/m^2. By setting this value to 0, the point cloud density can exceed 8000 points/m^2.

Distance Filtering: This value should be adjusted according to the height of the handheld device above the ground during field data collection. A minimum distance filter setting of 1.5 is recommended, as this value can generally eliminate human shadows. The results of the processing are illustrated in Figure 3.

3 Point cloud data preprocessing

3.1 Point cloud registration

3.1.1 Registration principle

Point cloud registration involves the use of appropriate translation and rotation matrices to perform rigid transformations of coordinate systems for data integration. Initially, the origin of the local coordinate system o-xyz is aligned with the origin of the global coordinate system O-XYZ. Subsequently, a rotational transformation is applied to the regional coordinate axes to ensure the alignment of the axes of the two coordinate systems. The registration transformation is based on the principles of rigid transformation, as detailed in Equations (3) and (4).

$$\begin{bmatrix} X \\ Y \\ Z \end{bmatrix} = \lambda R\left(\alpha, \beta, \gamma\right) \begin{bmatrix} x \\ y \\ z \end{bmatrix} + \begin{bmatrix} X' \\ Y' \\ Z' \end{bmatrix} \tag{3}$$

$$R(\alpha, \beta, \gamma) = \begin{bmatrix} A_{1,1} & A_{1,2} & A_{1,3} \\ A_{2,1} & A_{2,2} & A_{2,3} \\ A_{3,1} & A_{3,2} & A_{3,3} \end{bmatrix} \tag{4}$$

where $A_{1,1} = \cos\beta\cos\gamma$, $A_{1,2} = \cos\beta\sin\gamma$, $A_{1,3} = -\sin\beta$, $A_{2,1} = -\cos\alpha\sin\gamma + \sin\alpha\sin\beta\cos\gamma$, $A_{2,2} = \cos\alpha\cos\gamma + \sin\alpha\sin\beta\sin\gamma$, $A_{2,3} = \sin\alpha\cos\beta$, $A_{3,1} = \sin\alpha\sin\gamma + \cos\alpha\sin\beta\cos\gamma$, $A_{3,2} = -\sin\alpha\cos\gamma + \cos\alpha\sin\beta\sin\gamma$, $A_{3,3} = \cos\alpha\cos\beta$.

In Equation (3), $[X', Y', Z']$ and $R(\alpha, \beta, \gamma)$ represent the translation and rotation matrices, respectively, where λ is the scaling factor, and (α, β, γ) are the rotation angles. The six transformation parameters can be derived using the least squares method by substituting three common points.

3.1.2 Registration method

Manual registration requires the presence of distinctly overlapping regions with feature points when scanning the target object; otherwise, successful registration becomes challenging. The registration process relies on the identification of corresponding feature points and lines. A lack of distinct feature information can impede the recognition of these corresponding feature points and lines, consequently affecting the accuracy of the registration results. The registration outcome is illustrated in Figure 4.

Figure 4. Result of point cloud registration.

3.1.3 *Point cloud clipping*

While the point cloud data for the rocks is relatively good, the original scene is complex and contains a significant amount of noise, leading to confusion between the rocks and the background. Therefore, it is necessary to perform clipping to separate the data from the background. The clipping result is shown in Figure 5.

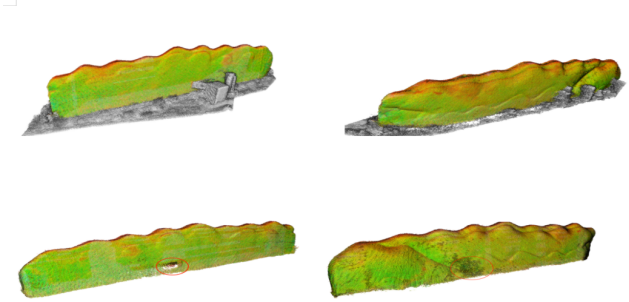

Figure 5. Clipping result of sculpted stone.

3.1.4 *Point cloud denoising*

This study primarily employs a statistical filter to remove outliers from the point cloud, which are often introduced by measurement noise. The working principle of statistical filtering is as follows: in 3D space, outliers are sparsely distributed and have a low information density, thus regarded as noise. By setting a threshold, outliers below this threshold are classified as invalid data. A statistical analysis is conducted within the neighborhood of each point, assuming that the distances of all points in the point cloud conform to a Gaussian distribution, characterized by the mean μ and standard deviation σ. Let the coordinates of the n-th point be $P_n(X_n, Y_n, Z_n)$, with the distance to any point $P_m(X_m, Y_m, Z_m)$ defined as:

$$S_i = \sqrt{(X_n - X_m)^2 + (Y_n - Y_m)^2 + (Z_n - Z_m)^2} \quad (5)$$

The average distance formula for traversing all points to any point is given by:

$$\mu = \frac{1}{n} \sum_{i=1}^{n} S_i \quad (6)$$

The standard deviation is calculated as follows:

$$\sigma = \sqrt{\frac{1}{n} \sum_{i=1}^{n} (S_i - \mu)^2} \quad (7)$$

Let the standard deviation multiplier be std. By inputting the thresholds k and std a point is retained if its average distance to k neighboring points falls within the standard range $(\mu - \sigma \cdot \text{std}, \mu + \sigma \cdot \text{std})$; otherwise, it is classified as an outlier and deleted.

The results of the statistical filtering are presented in Figure 6, while the noise points removed during the process are shown in Figure 7.

Figure 6. Processing results with $k = 5$ and std $= 4$.

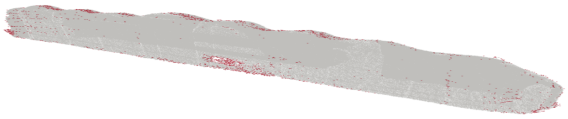

Figure 7. Illustration of noise removal (Red) using statistical filtering.

3.2 Data quality evaluation

The objective of point cloud quality evaluation is to automate the assessment of the visual quality of point clouds after various distortions have been introduced.

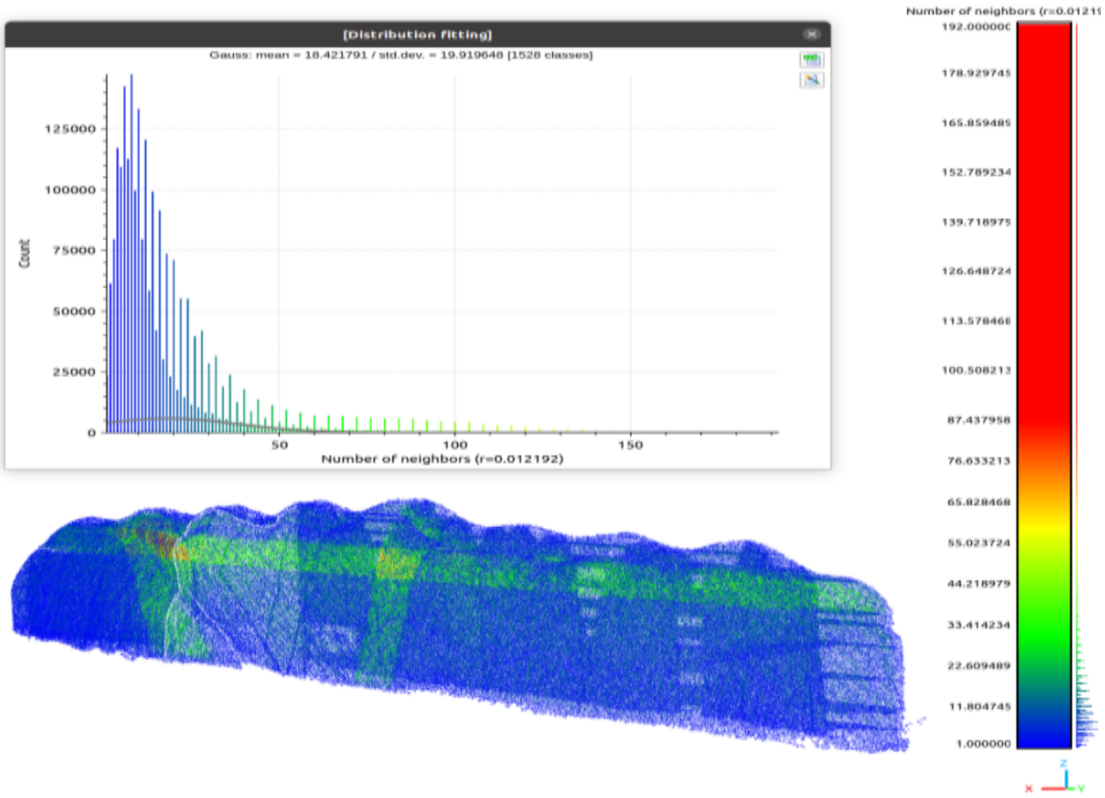

Figure 8. Point density evaluation.

3.2.1 *Point cloud density*

Point cloud density is a crucial attribute that reflects the spatial distribution and density of the laser point cloud, thereby directly indicating the spatial distribution characteristics of the target object. The k-nearest neighbor (kNN) algorithm is a fundamental method for classification and regression. Its basic principle involves evaluating the density of a sample point by calculating the number of its k nearest neighbors. The common approach to compute point density is to count the number of sample points within a specified radius. The higher the number of sample points within this range, the greater the density of the sample point. As shown in Figure 8, with a neighborhood radius of 0.012192, the point density calculated using the kNN algorithm is 18.42.

3.2.2 *Roughness*

Surface roughness quantifies microscopic irregularities, involving minute spacing and fluctuations between peaks and valleys, characterizing geometric deviations at the micro level. A smaller roughness value indicates a smoother surface. The k-nearest neighbor algorithm is employed to compute roughness, which evaluates the roughness of a sample point by calculating the inconsistency of the labels of its k nearest neighbors. Specifically, for each sample point, the algorithm identifies its k nearest sample points and assesses the degree of label inconsistency among them. As shown in Figure 9, with a neighborhood radius of 0.012192, the roughness calculated using the k-N algorithm is 0.012.

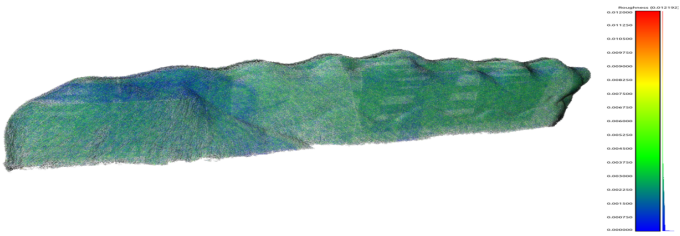

Figure 9. Roughness evaluation.

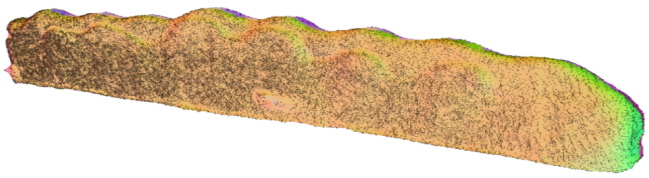

Figure 10. Visualization of point cloud data and model.

4 3D point cloud reconstruction

3D point cloud reconstruction refers to the process of restoring the surface or contour of an object based on 3D point cloud data, commonly known as surface reconstruction. A 3D point cloud consists of a collection of discrete points that have

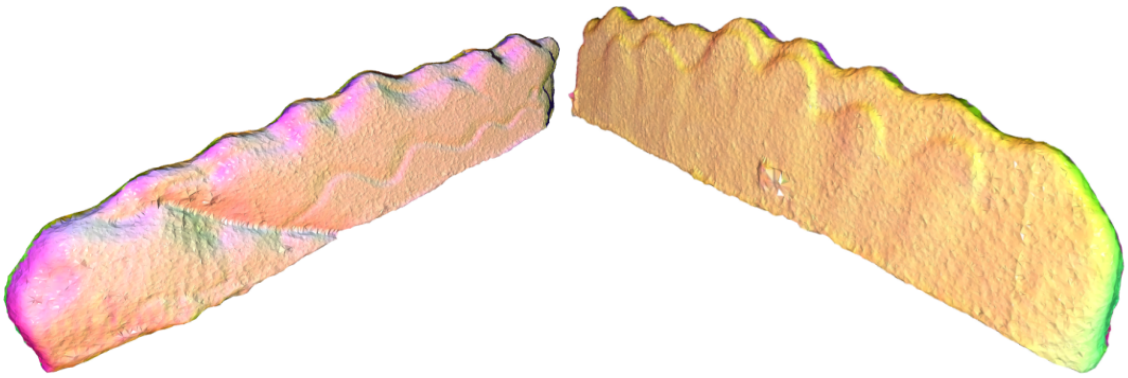

Figure 11. Reconstruction effect at $\alpha = 0.1$.

certain gaps between them, resulting in some spatial locations lacking direct data information. Through the processing and interpolation of these discrete points, 3D reconstruction creates surfaces composed of smoothly transitioning planar or curved elements, thus achieving continuity and integrity of the object's surface. This ensures that the reconstructed result can accurately reflect the form and details of the original object.

4.1 Point cloud modeling

4.1.1 Alpha shapes reconstruction

The Alpha-shape algorithm has applications in point cloud modeling. Jang et al. [13] constructed various 3D models of tree canopies by adjusting the parameter α. For the object of study in this paper, As shown in Figures 10 and 11, a carefully selected parameter α is employed to fit the various sections of the point cloud data, enabling rapid capture of spatial morphology and the construction of an accurate spatial model.

4.1.2 Ball pivoting reconstruction

The Ball Pivoting Algorithm (BPA) is an effective method for reconstructing the surfaces of point cloud data. After setting a ball radius r, when the sphere rolls and contacts the points without any other points inside, a triangle is formed with the axis of rotation. As shown in Figure 12, BPA begins with a seed triangle, and the sphere rotates along the edges to contact new points, thereby forming new triangles.

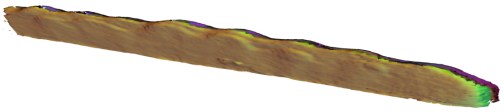

Figure 12. Presence of holes when radii = [0.1, 0.2, 0.4, 0.6].

4.1.3 Poisson surface reconstruction

Poisson reconstruction is an advanced method for constructing 3D surfaces that can transform a discrete set of 3D points into a continuous and watertight triangular mesh network [14].

For an object N and its boundary ∂N the indicator function χ and fundamental functions F are defined as shown in Equations (8), (9), and (10).

$$\chi_N(x) = \begin{cases} 1 & x \in N \\ 0 & x \notin N \end{cases} \tag{8}$$

$$F(x, y, z) \equiv (B(x)B(y)B(z))^{*n} \tag{9}$$

$$B(t) = \begin{cases} 1 & |t| < 0.5 \\ 0 & \text{Others} \end{cases} \tag{10}$$

The point cloud data is divided using an octree, and the points within each node are processed using Equation (11).

$$F_o(q) = F\left(\frac{q - o.c}{o.w}\right)\frac{1}{o.w^3} \tag{11}$$

The gradient space is approximated using the function represented in Equation (12), where Ω denotes the scatter set, ss indicates the K-nearest neighborhood of a point in the scatter set, and α, o, s are interpolation weights with s. N as the vertex normal vector.

$$V(q) \equiv \sum_{s\in\Omega}\sum_{o\in D(s)} \alpha_{o,s} F_o(q) s.N \tag{12}$$

The Poisson equation is solved to derive the indicator function χ using Equation (13).

$$\sum_{o\in\mathcal{G}} |\langle \triangle\chi - \nabla V, F_o\rangle|^2 = \sum_{o\in\mathcal{G}} |\triangle\chi, F_o - \nabla V, F_o|^2 \tag{13}$$

Finally, As shown in Figures 13 and 14 the isosurface is extracted using the moving cubes method, followed by the connection of triangular patches to yield the reconstructed surface.

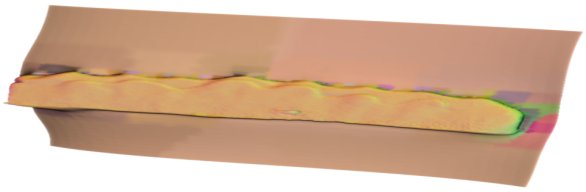

Figure 13. Original effect of poisson reconstruction showing severe distortion.

Figure 14. Model after clipping from poisson reconstruction.

4.1.4 Greedy projection triangulation reconstruction

This algorithm is based on the incremental surface growth principle and follows a greedy approach. The algorithm proceeds as follows:

Input point q and determine its k nearest neighbor points through KD-tree search, classifying the point cloud into free points, completed points, edge points, and boundary points.

Determine the projection tangent plane for q and its neighboring points, projecting these points onto a two-dimensional plane.

As shown in Figure 15, in the two-dimensional plane, apply the greedy projection algorithm for triangulation, selecting locally optimal expansion points, and map them back to 3D space through projection relationships. This process is repeated until the surface reconstruction of the object is complete.

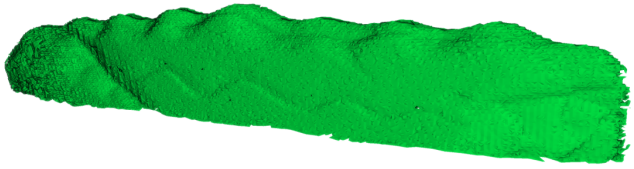

Figure 15. Modeling effect of the greedy triangulation algorithm.

5 Surface area calculation and analysis

5.1 Surface area measurement

5.1.1 Traditional measurement methods

1. Steel tape measurement estimation method

The steel tape measurement technique involves first measuring the dimensions of the outer rectangular projection of the artificial hill on both the horizontal and vertical planes, followed by calculating the area of these two projection surfaces. Finally, a conversion factor is applied to estimate the surface area of the artificial stone hill. Let S represent the estimated surface area and α denote the area conversion coefficient, which typically ranges from 1.3 to 2.2.

2. Paper patch method

The paper patch method involves closely adhering sheets of paper to the surface of the artificial hill until it is completely covered. Subsequently, by counting the number of sheets used and determining the area of each sheet, the surface area of the artificial hill can be accurately calculated through appropriate mathematical operations. Let n denote the number of sheets and S represent the area of a single sheet. Using these two methods, the surface areas of the artificial stone were measured as 15.2 m^2 and 10.7 m^2, respectively.

5.1.2 Surface area measurement based on 3D laser scanning technology

The convex hull is a polyhedron where all internal angles are less than or equal to 180 degrees. The calculation of its area is influenced by factors such as mesh resolution and surface smoothness. If the mesh is very coarse or contains many small triangles, the calculated surface area may be slightly larger than the actual value. Conversely, if the mesh is overly smooth, some details may be lost, leading to an underestimation of the surface area.

The general steps for calculating the surface area of the convex hull using the Open3D library are as follows:

(1) Obtain the convex hull

Table 1. Experimental results analysis.

Measurement Method	Surface Area (m^2)	Time Consumed (h)	Measurement Accuracy	Workload	Technical Difficulty	Applicability
Steel Tape Measurement Method	15.2	1	Low	Small	Easy	Engineering Estimation
Paper Patch Method	10.7	2	High	Very Large	Easy	Small Area Measurement
3D Laser Scanning Technology	10.338	0.5	High	Smaller	Relatively Difficult	Indoor or Low Height Areas

Acquire the triangular mesh generated through surface reconstruction algorithms.

(2) Traverse the triangular faces of the convex hull

The convex hull is typically composed of a series of triangular faces.

(3) Calculate the area of each triangle

Determine the coordinates of the three vertices of each triangle and use these coordinates to calculate the normal vector and edge vectors, thereby obtaining the area.

(4) Accumulate the areas of all triangles

Summing the areas of all triangles yields the surface area of the convex hull.

Using this method, the calculated surface area is 10.337555962374813 m^2.

5.2 Results

Although the steel tape measurement estimation method is commonly used in quantity estimation for engineering projects, the irregular shape of objects poses significant challenges for precise area measurement, resulting in considerable error. In contrast, the paper patch method, characterized by its simplicity and high accuracy, performs exceptionally well in calculating the surface area of small-scale artificial stone projects; however, this method can be time-consuming and labor-intensive. The introduction of 3D laser scanning technology offers high precision, strong confidence, and efficiency, making it feasible for calculating the surface areas of irregularly shaped objects. The experimental results are summarized in Table 1.

6 Conclusion

This paper highlights the advantages of 3D laser scanning technology for accurately and quickly measuring the surface area of irregularly shaped objects like artificial stone. It details the measurement process, data collection, and the effectiveness of various reconstruction algorithms, demonstrating significant reductions in measurement time and high-density data acquisition. While the study establishes a strong foundation for using this technology, it acknowledges limitations in precision, the need for standardized evaluation methods, and a limited sample size for broader applicability. Overall, 3D laser scanning shows promise for surface area measurement, but further research is needed to improve its precision and universality.

Conflicts of Interest

The authors declare no conflicts of interest.

Funding

This work was supported without any funding.

References

[1] El-Hakim, S. F., Brenner, C., & Roth, G. (1998). A multi-sensor approach to creating accurate virtual environments. ISPRS journal of photogrammetry and remote sensing, 53(6), 379–391.

[2] Lemmens, M. (2023). Airborne and Ground-based Laser Scanning. In *The Routledge Handbook of Geospatial Technologies and Society* (pp. 171-187). Taylor and Francis.

[3] Yu, Y., Ferencz, A., & Malik, J. (2001). Extracting objects from range and radiance images. IEEE Transactions on Visualization and Computer Graphics, 7(4), 351–364. [CrossRef]

[4] Allen, P. K., Stamos, I., Troccoli, A., Smith, B., Leordeanu, M., & Hsu, Y. C. (2003, September). 3D modeling of historic sites using range and image data. In *2003 IEEE International Conference on Robotics and Automation* (*Cat. No. 03CH37422*) (Vol. 1, pp. 145-150). IEEE. [CrossRef]

[5] Abergel, V., Manuel, A., Pamart, A., Cao, I., & De Luca, L. (2023). Aïoli: A reality-based 3D annotation cloud platform for the collaborative documentation of cultural heritage artefacts. *Digital Applications in Archaeology and Cultural Heritage*, 30, e00285.[CrossRef]

[6] Lifeng, Z. H. A. O., Chao, T. A. N. G., & Haiqian, H. O. U. (2020). Intelligent diagnosis technology and service status evaluation of rail transit tunnel. *Bulletin of Surveying and Mapping*, (9), 1.

[7] Zhao, D., Liu, C., Zhang, X., Zhai, X., Deng, Y., Chen, H., ... & Luo, P. (2023). 3D digital modeling as a sustainable conservation and revitalization path for the cultural heritage of han dynasty stone reliefs. *Sustainability*, 15(16), 12487. [CrossRef]

[8] Ellmann, A., Kütimets, K., Varbla, S., Väli, E., & Kanter, S. (2022). Advancements in underground mine surveys by using SLAM-enabled handheld laser scanners. *Survey Review*, 54(385), 363-374. [CrossRef]

[9] Parfenov, V., Igoshin, S., Masaylo, D., Orlov, A., & Kuliashou, D. (2022). Use of 3D laser scanning and additive technologies for reconstruction of damaged and destroyed cultural heritage objects. Quantum Beam Science, 6(1), 11. [CrossRef]

[10] Dawei, Z., Lizhuang, Q., Demin, Z., Baohui, Z., & Lianglin, G. (2020). Unmanned aerial vehicle (UAV)

photogrammetry technology for dynamic mining subsidence monitoring and parameter inversion: A case study in China. *IEEE Access*, 8, 16372-16386. [CrossRef]

[11] Edelsbrunner, H., Kirkpatrick, D., & Seidel, R. (1983). On the shape of a set of points in the plane. *IEEE Transactions on information theory*, 29(4), 551-559. [CrossRef]

[12] Li, L., & Yan, H. (2021, June). Building contour regularization method based on ground LIDAR point cloud data. In *2021 IEEE 4th Advanced Information Management, Communicates, Electronic and Automation Control Conference* (IMCEC) (Vol. 4, pp. 1937-1941). IEEE.[CrossRef]

[13] Jang, E., & Kang, W. (2023). Estimating Riparian Vegetation Volume in the River by 3D Point Cloud from UAV Imagery and Alpha Shape. *Applied Sciences*, 14(1), 20. [CrossRef]

[14] Kazhdan, M., & Hoppe, H. (2023, September). Distributed poisson surface reconstruction. In *Computer Graphics Forum* (Vol. 42, No. 6, p. e14925). [CrossRef]

Quan Qi Currently majoring in computer science and engineering in College of Information Science and Engineering, Henan University of Technology. The research direction is remote sensing in sea ice concentration. (Email: 435995612@qq.com)

Xingdong Wang Currently working at the School of Information Science and Engineering, Henan University of Technology. The research direction is software development and GIS (geographic information system).
(Email: zkywxd@163.com)

Yuhua Wang Currently working at the School of Information Science andEngineering, Henan University of Technology. The research direction is intelligent control and information security. (Email: 9109348@qq.com)